iScience

CellPress
OPEN ACCESS

Article

A robotic system for real-time analysis of inhaled submicron and microparticles

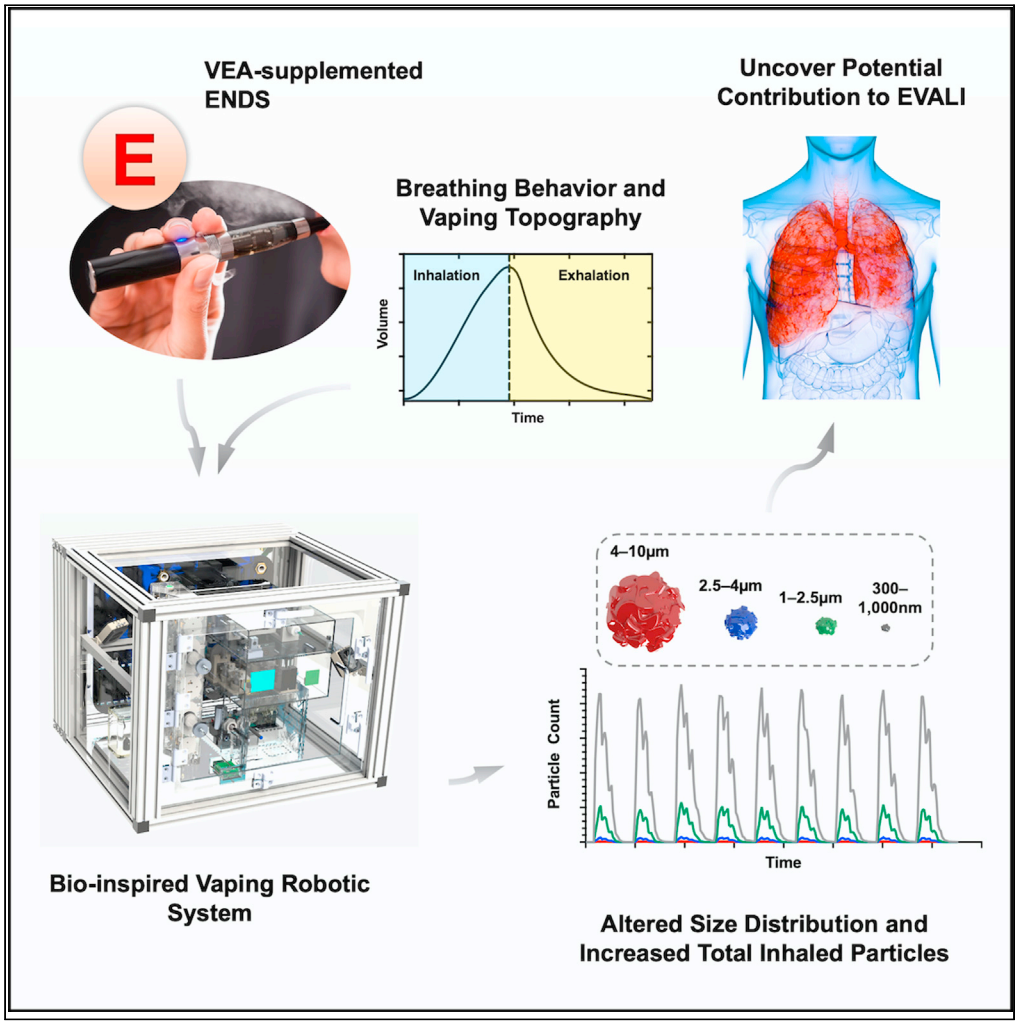

Alexander J. Kaiser, Cassie Salem, Bob J. Alvarenga, Anthony Pagliaro, Kelly P. Smith, Luis G. Valerio, Jr., Kambez H. Benam

benamk@pitt.edu

Highlights

Vitamin E acetate (VEA) has been strongly linked to outbreak of EVALI

A bio-inspired robot was created for real-time analysis of inhaled particles from ENDS

VEA in e-liquid, even at small doses, was sufficient to enhance total inhaled particles

This robotic system enables preclinical toxicity evaluation of ENDS and tobacco products

Kaiser et al., iScience 24, 103091
October 22, 2021
https://doi.org/10.1016/j.isci.2021.103091

iScience

CellPress
OPEN ACCESS

Article

A robotic system for real-time analysis of inhaled submicron and microparticles

Alexander J. Kaiser,[1] Cassie Salem,[1] Bob J. Alvarenga,[1] Anthony Pagliaro,[1] Kelly P. Smith,[1] Luis G. Valerio, Jr.,[2] and Kambez H. Benam[3,4,5,6,*]

SUMMARY

Vitamin E acetate (VEA) has been strongly linked to outbreak of electronic cigarette (EC) or vaping product use-associated lung injury. How VEA leads to such an unexpected morbidity and mortality is currently unknown. To understand whether VEA impacts the disposition profile of inhaled particles, we created a biologically inspired robotic system that quantitatively analyzes submicron and microparticles generated from ECs in real-time while mimicking clinically relevant breathing and vaping topography exactly as happens in humans. We observed addition of even small quantities of VEA was sufficient to alter size distribution and significantly enhance total particles inhaled from ECs. Moreover, we demonstrated utility of our biomimetic robot for studying influence of nicotine and breathing profiles from obstructive and restrictive lung disorders. We anticipate our system will serve as a novel preclinical scientific research, decision-support tool when insight into toxicological impact of modifications in electronic nicotine delivery systems is desired.

INTRODUCTION

Over the past decade, the use of electronic nicotine delivery systems (ENDSs), such as electronic cigarettes (ECs), has surged. In addition to health concerns for healthy adults, the use of ENDSs among the youth population and those with underlying lung conditions is particularly of concern (Overbeek et al., 2020; Bowler et al., 2017). Since 2018, serious pulmonary adverse effects from use of ENDS have been noted to be the rise. In 2019, the United States Centers for Disease Control and Prevention (CDC) and the Food and Drug Administration (FDA) began investigating a national outbreak of EC or vaping product use-associated lung injury (EVALI) (Reagan-Steiner et al., 2020). EVALI led to hospitalizations, as a result of serious acute to subacute lung injury, and fatalities. Alpha-tocopheryl acetate (also known as vitamin E acetate [hereafter referred to as VEA]), a dietary compound discovered to be used a diluent in some cannabis-containing ECs and vaping products, has been strongly linked with the EVALI outbreak (Blount et al., 2020; Krishnasamy et al., 2020; Duffy et al., 2020). Thus far, the specific cause(s) of EVALI is unknown; however, the analyses of products and patient samples have implicated a role for VEA. Despite this, studies on how VEA can lead to EVALI have been sparse and limited to inhalation exposure of laboratory murine models to EC aerosols (Bhat et al., 2020), challenging human bronchial and monocytic leukemia-derived cell lines with EC liquid (e-liquid) (Muthumalage et al., 2020), or focused on solubility and thermal decomposition of VEA (Wu and O'Shea, 2020; Kozlovich et al., 2021).

Here, we sought to identify a VEA-associated physical signature in the aerosol of what a human would inhale from use of an EC. More specifically, we asked whether the presence of VEA can impact the profile and quantity of particles generated from ECs when exactly recreating clinically relevant breathing profiles and vaping topography that are observed in human subjects. Such information will quantitatively improve the understanding of the interactions of particles emitted from ENDS aerosols upon the airway and lung tissue because of ENDS use. This information may be able to be used to help characterize the potential toxicity of aerosolized compounds on pulmonary tissues to support constituent and product assessments. Thus, this study describes the design and development of a first-in-kind biologically inspired robotic system that generates fresh aerosols for any desired EC in a very controlled and user-definable manner and subsequently utilizes an optical sensing system to quantitate and analyze submicron and microparticles (300 nm–10 μm in 4 segmented ranges) from every puff over the course of vaping session in real-time. The addition of as little as 1.25% VEA was observed to be sufficient to significantly enhance total particles

[1]Department of Bioengineering, University of Colorado Denver, Aurora, CO 80045, USA

[2]Division of Nonclinical Science, Office of Science, Center for Tobacco Products, U.S. Food and Drug Administration, Silver Spring, MD 20993, USA

[3]Division of Pulmonary, Allergy and Critical Care Medicine, Department of Medicine, University of Pittsburgh, Pittsburgh, PA 15213, USA

[4]Department of Bioengineering, University of Pittsburgh, Pittsburgh, PA 15219, USA

[5]Vascular Medicine Institute, University of Pittsburgh, Pittsburgh, PA 15213, USA

[6]Lead contact

*Correspondence: benamk@pitt.edu

https://doi.org/10.1016/j.isci.2021.103091

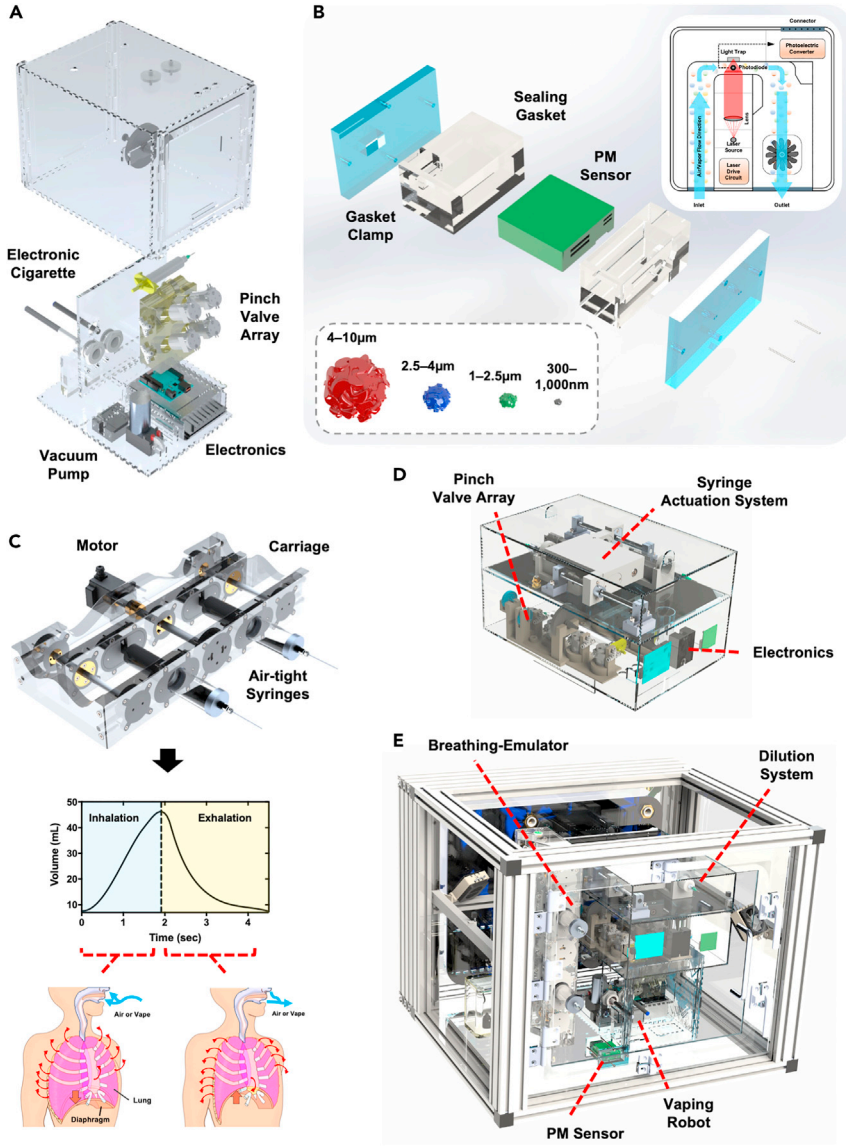

Figure 1. Experimental setup and technology overview

(A) The vaping robot is responsible for activating electronic cigarettes (ECs) and capturing the aerosols into a reservoir from which the breathing-emulator inhales. The system consists of ECs connected to an array of pinch valves, through a sealed custom gasket, which are responsible for fluidically connecting and disconnecting lines to allow for the proper flow depending on the current state of the system. An onboard vacuum pump is responsible for pulling the EC aerosols into the reservoir. All of the functionality of the vaping robot is controlled by a microcontroller and a series of relays and is powered with an onboard power supply.

(B) The inline particulate matter sensor is responsible for detecting the quantities of particles passing through the system that are categorized into four different particle size ranges, the smallest particle size group is from 300 nm–1 μm, then 1 μm–2.5 μm, 2.5 μm–4 μm, and as the largest 4 μm–10 μm. The PM sensor is a laser-based technology that utilizes optical diffraction produced from the passing particles. The PM sensor is contained within a custom airtight gasket and is sealed by pressure applied to the gaskets through the gasket clamps, where one side of the clamp has two ports which link the breathing-emulator and the vaping Robot.

(C) The breathing-emulator mimics physiological breathing through actuating plungers of air-tight syringes that are mounted to the carriage of the system. The breathing-emulator is programmed with a clinically relevant breathing profile that gives a dynamic flow rate through actuating the movement of the plungers at a dynamic velocity. When the plungers are retracted the breathing-emulator is inhaling and when compressed the breathing-emulator is exhaling.

(D) The dilution robot contains onboard electronics, a series of pinch valves and filters, a vacuum pump, and a mechanical actuation system for driving two 30 mL syringes. It sits on top of the vaping robot and connects to it via its two fluidic

Figure 1. *Continued*
connections. The system can be programmed to dilute the aerosols collected by the vaping robot at any specified factor. The dilution robot's dilution profile is synchronized with the vaping robot's vaping regiment so that dilution occurs and ends within the appropriate time (after the vaping robot's puff but before the inhalation of the aerosols). (E) The Inhalation exposure chamber is a custom-engineered system that controls the internal atmosphere conditions by sensing and regulating humidity, carbon dioxide, and temperature. It is purposefully designed to house all the other hardware used for the experiments (A–D), including the breathing-emulator, the iInline PM sensor, the vaping robot, and the dilution robot.

inhaled from an EC. Interestingly, nicotine levels inversely yet non-significantly correlated with particles generated from ECs. However, addition of VEA led to significant increase in submicron and microparticles in aerosols of ECs containing 0.6% nicotine. Lastly, by emulating representative breathing profiles from obstructive and restrictive lung disorders, we identified a similar trend in ability of VEA to enhance particles quantities in inhaled aerosols, which reveals potential inhaled toxicity due to VEA in conditions such as chronic obstructive pulmonary disease (COPD) and idiopathic pulmonary fibrosis (IPF). To our knowledge, no such system with this level of sophistication, programmability and real-time sensing for inhaled aerosols physical characterization has been developed, and our platform offers the unique ability to study the effects of any desired chemical constituent of ECs on inhaled submicron and microparticles for clinical correlation. In fact, real-time detection system may have considerable applications for scientific and regulatory science purposes.

RESULTS

Design and development of a human vaping mimetic real-time submicron and microparticle analyzer

To enable studies on impact of chemical constituents of EC (such as VEA and nicotine) and breathing profile (healthy and diseased) on inhaled particle quantities and distribution, we developed a first-in-kind human vaping mimetic real-time submicron and microparticle analyzer (Figure 1). This platform consists of multiple inter-linked subsystems responsible for controlling the experimental environment, emulating physiologically relevant airflow dynamics and clinical vaping topography, and analyzing particles in segmented distributions over relevant particle sizes.

We initially designed and assembled a vaping robot (Figures 1A, S1, and S2) that is responsible for "vaping" ECs in a clinically relevant manner. This system is an enhanced and EC-focused iteration of a cigarette smoking machine that we had developed earlier (Benam et al., 2016a, 2020) and functions by activating placed-in ECs through negative pressure for a programmed (user-defined) duration of time – i.e., puff time, to fill in a user-selected reservoir – i.e., puff volume, with freshly produced EC aerosols. In our studies we set the puff time and volume to 3 s and 55 mL, respectively. These values were selected based on the 2018 International Organization for Standardization (ISO) definitions and standard conditions for vapor productions ISO 20768:2018 (ISO 20768:2018, 2018). The vaping robot is concurrently connected to an inline particulate matter (PM) Sensor located within a purposely built air-tight enclosure (Figures 1B and S3), which in turn is linked to a custom-designed and engineered breathing-emulator (Figures 1C and S4). The PM Sensor is laser-based and allows for detection of particles ranging from 300 nm to 10 μm (the choice of Sensor in our platform was made after thorough comparison against existing commercially available detection systems; see discussion below). The Breathing-Emulator rhythmically "inhales" and "exhales" air or aerosols by following breathing patterns and volumes dictated by input profiles. For our studies, we utilized healthy normal breathing. The vaping robot is highly versatile and allows generation of fresh whole aerosols from any desired buttonless EC (by allowing use of mouth-piece gaskets, that based on dimensions of an EC, conform tightly, and create an air-tight seal) while synchronizing operation with the Breathing-Emulator. (For ECs that are not automatically activated by the negative pressure and require simultaneous activation by user through pressing a button on the device, we would need to design, build, and integrate an additional module to mechanically press the device button at the time of negative pressure.) Between the time that an EC is activated to produce fresh aerosols and when the puff of aerosols is to be sampled and analyzed by the PM sensor under inhalation fraction of rhythmic breathing, the aerosols get diluted with the dilution robot (Figures 1D and S5). This is to recapitulate the dilution that occurs after an EC-smoker smoothly inhales a puff of vapor/aerosol (e.g., 55 mL) at a flat flow rate – i.e., using square-shape puffing profile. Experimentally, this is executed through constant vacuum pressure of the vaping robot for the duration of puff and mixed with tidal volume-equivalent air (e.g., 500 mL which represents the

volume that an average adult human breathes at resting state) for dynamic delivery to the lungs. The dilution robot is linked to the vaping robot's internal reservoir. Following fresh puff generation, the dilution robot takes in the aerosol from the reservoir and runs it through a seamless and quick series of filtered air addition, mixing, sampling, and re-diluting steps (if required) (Figures S6 and S7). The platform was designed so that the user, based on the question of study, can create dilution of interest. Here, to reproduce clinically relevant exposure, we programmed the dilution robot to generate 10-fold dilution of each inhaled EC puff. Additionally, we recapitulate physiologically relevant body temperature and added humidity. Lastly, we developed an inhalation exposure chamber (Figures 1E, S8, and S9) that houses all the above subsystems and automatically senses and regulates the environmental conditions via values set forth by user and, through a set of pressure-controlling pneumatics, can safely exhaust unneeded aerosols out of the system. In our studies, we set the relative humidity (RH) at 70% (the maximum that our chamber allowed without negatively impacting electronics and mechanical parts) and the temperature at 37°C (Figures S10–S15).

Evaluating impact of supplemental VEA on inhaled particle profiles from EC

Next, to evaluate the effects of VEA on aerosol particle size distributions during vaping, we prepared increasing concentrations of VEA (0%, 1.25%, 2.5%, and 5% (v/v)) in 50/50 solution of propylene glycol/vegetable glycerin (PG/VG). Each condition (e-liquid) was then loaded into an EC cartridge, which was connected to a battery and plugged into the vaping robot within the inhalation exposure chamber (Figure 1). Following EC loading, the system was initiated with a representative vaping session of 9 total puffs at 41.3-s inter-puff intervals and 3-s puff times. During the 41.3 s, a total of seven inhalation-exhalation cycles occurred; one over the course of the puff followed by six during the post-puff period, all at a rate of 5.9 s per puff or breath.

During the vaping session, the PM sensor monitored and analyzed the distribution of particles in real-time, categorizing them into four segmented ranges of 300 nm–1 μm, 1 μm–2.5 μm, 2.5 μm–4 μm, and 4 μm–10 μm (Figure 2A). The analysis was performed through a custom-developed companion software that calculates the peak total particles counted per cm^3 over the course of each individual (diluted) puff. We collected data for seven independent vaping sessions, that is a total of 63 puffs, and analyzed them to get insight into the impact of VEA and its dose on the four particle distribution profiles (Figure 2B). The results demonstrate statistically significant differences in all the VEA concentrations for all particle size distributions other than 1.25% vs. 2.5%. A relatively similar trend was also evident when analyzing peak concentration for submicron and microparticles (Figure S16). In addition, we summed together the total particles counted per cm^3 over the seven vaping sessions for each VEA concentration (Figure 3) and observed that the total collective particles went up as VEA concentration increased, with the highest quantity seen at 5% dose. Interestingly, the percentage of submicron particles (300 nm–1 μm fraction) out of the total of all fractions within each condition slightly decreased with increase in VEA, whereas the percentage of particles within the 1 μm–2.5 μm and 2.5 μm–4 μm fractions enhanced with increase in the VEA dose. We found no change in fraction of 4 μm–10 μm particles with increased concentration of VEA. To ensure the PM sensor is not saturated for signal detection, we performed serial dilutions of 5% VEA and observed a relatively linear change in particle count and concentration as the solution got more diluted (Figure S17). This graph also validates our optical-based aerosol sensing approach as changes made (by dilution) in input sample are reflected by anticipated total particle counts.

Effects of nicotine on inhaled particle profiles from EC, alone or in combinatorial mixture with VEA

We next aimed to determine the effects on the particle size distribution in the presence of varying concentrations of nicotine – an additive in many EC and vaping products, alone and in combination with VEA. The 50/50 PG/VG was used as base to dissolve VEA at 0% or 5% (v/v) doses. Each of these solutions were then independently mixed with purified (−)-nicotine to yield 0%, 0.6%, 1.2%, and 2.4% (wt/v) concentrations. We studied these e-liquids using the same breathing profile, vaping topography, and other parameters applied in our studies above (9 puffs per vaping session totaling to 63 puffs over seven vaping sessions, 55 mL puff volume, 3-s puff time, 41.3-s inter-puff interval, 10X puff dilution, 37°C, and healthy adult breathing inhale/exhale cycle of 5.9 s).

The total particles counted per cm^3 were calculated from the raw data produced from the vaping sessions (Figure 4). The data showed a statistically significant difference between the 0% and 5% VEA at both 0%

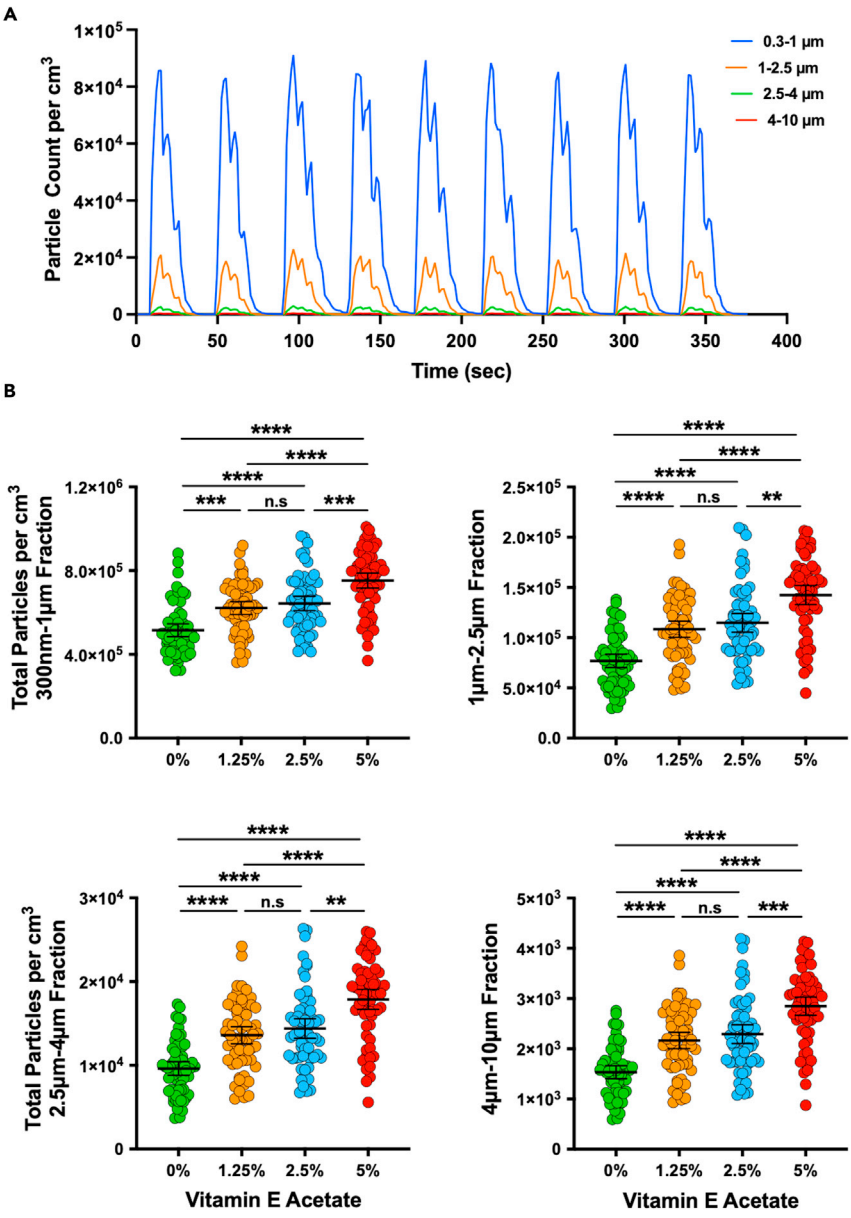

Figure 2. Impact of vitamin E acetate (VEA) on inhaled particle count

(A) Real-time particle count (per cm^3) as a function of time for four particle size distributions (300 nm–1 μm, 1 μm–2.5 μm, 2.5 μm–4 μm, and 4 μm–10 μm) during 9 cycles of the vaping session is illustrated. The data were generated from representative e-liquid containing VEA at 5% (v/v) concentration in 50/50 propylene glycol/vegetable glycerin (PG/VG). (B) Distribution profiles of the total particle counts per cm^3 over each inter-puff interval for each size fraction (300 nm–1 μm, 1 μm–2.5 μm, 2.5 μm–4 μm, and 4 μm–10 μm) in the absence or presence of increasing doses of VEA (v/v at 0%, 1.25%, 2.5%, and 5%) are plotted. Kruskal-Wallis test demonstrated statistical significance ($p < 0.0001$), and post-hoc analysis (Dunn's multiple comparison test) showed statistically significant differences between all data sets except 1.25% and 2.5% for all particle size distributions. Error bars indicate mean and 95% confidence intervals for each data set.

(consistent with findings in Figures 2B) and 0.6% nicotine; however, statistical significance was not detected between the 0% and 5% VEA at higher (1.2% and 2.4%) nicotine concentrations. In fact, as the nicotine concentration increased, in both VEA-containing and VEA-free groups we identified a decrease (although not significant) in total particles counted per puff. A similar pattern was also evident when analyzing peak concentration for submicron and microparticles (Figure S18). We also summed the total particles counted per

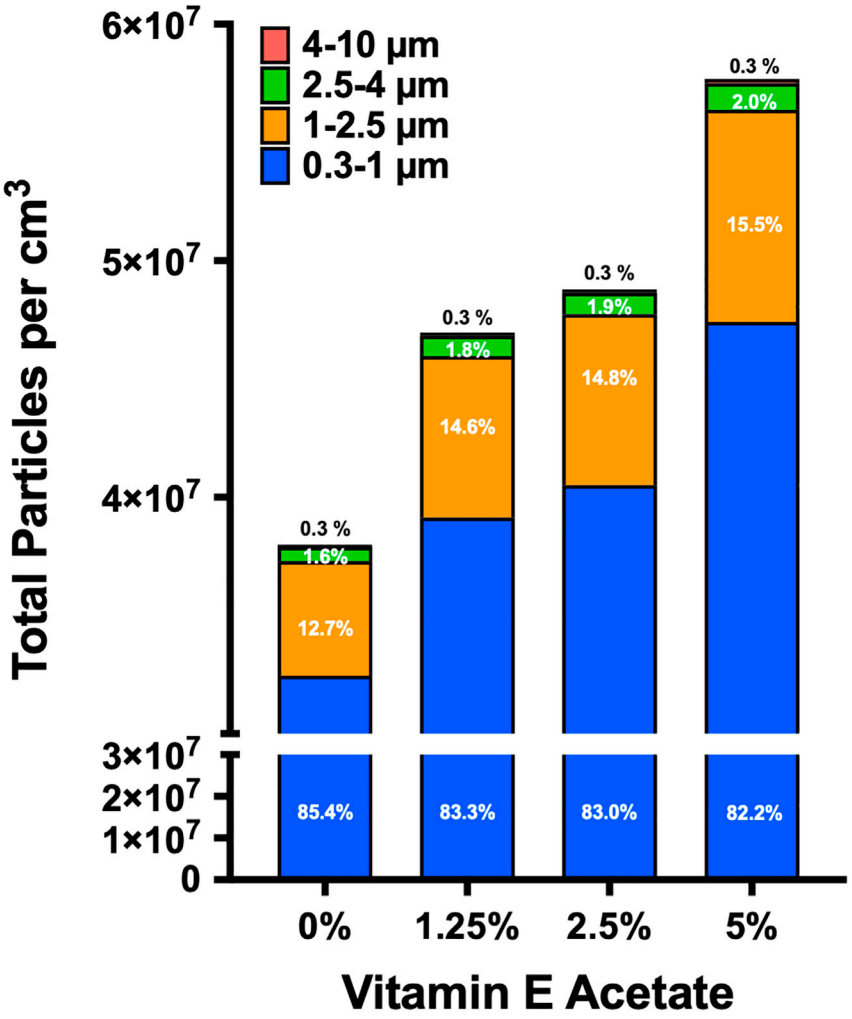

Figure 3. Impact of varying doses of electronic cigarette vitamin E acetate content on cumulative total submicron and microparticles inhaled over a representative vaping regiment

Total combined particles per cm^3 were counted at a sampling rate of 1.3 s over the course of seven independent vaping sessions (at 9 puffs per session) in the presence of a range of VEA concentrations (0%–5% v/v in 50/50 PG/VG). For each condition, the particle distribution size profile was segmented to display relative measured abundance of each size fraction as a percentage of total particles that were counted. The 0% VEA yielded 3.25×10^7 particles/cm^3 within 300 nm–1 µm (85.4% of total), 4.84×10^6 particles/cm^3 within 1 µm–2.5 µm (12.7% of total), 6.05×10^5 particles/cm^3 within 2.5 µm–4 µm (1.6% of total), and 9.65×10^4 particles/cm^3 within 4 µm–10 µm (0.3% of total). The 1.25% VEA yielded 3.91×10^7 particles/cm^3 within 300 nm–1 µm (83.3% of total), 6.83×10^6 particles/cm^3 within 1 µm–2.5 µm (14.6% of total), 8.56×10^5 particles/cm^3 within 2.5 µm–4 µm (1.8% of total), and 1.36×10^5 particles/cm^3 within 4 µm–10 µm (0.3% of total). The 2.5% VEA yielded 4.05×10^7 particles/cm^3 within 300 nm–1 µm (83.0% of total), 7.23×10^6 particles/cm^3 within 1 µm–2.5 µm (14.8% of total), 9.07×10^5 particles/cm^3 within 2.5 µm–4 µm (1.9% of total), and 1.44×10^5 particles/cm^3 within 4 µm–10 µm (0.3% of total). The 5% VEA yielded 4.74×10^7 particles/cm^3 within 300 nm–1 µm (82.2% of total), 8.97×10^6 particles/cm^3 within 1 µm–2.5 µm (15.5% of total), 1.13×10^6 particles/cm^3 within 2.5 µm–4 µm (2.0% of total), and 1.79×10^5 particles/cm^3 within 4 µm–10 µm (0.3% of total).

cm^3 over the seven vaping sessions for each VEA/nicotine combination (Figure S19). The cumulative total particle count was highest with 5% VEA at 0% and 0.6% nicotine concentrations. Interestingly, unlike the impact of VEA alone, as the nicotine dose increased (with or without presence of VEA) the percentage of particles in 300 nm–1 µm fraction for each condition slightly went up, while the percentage of particles within the 1 µM–2.5 µm and 2.5 µm–4 µm fractions moved in the opposite direction. We did not observe changes to optical opacity of aerosols at VEA doses we tested.

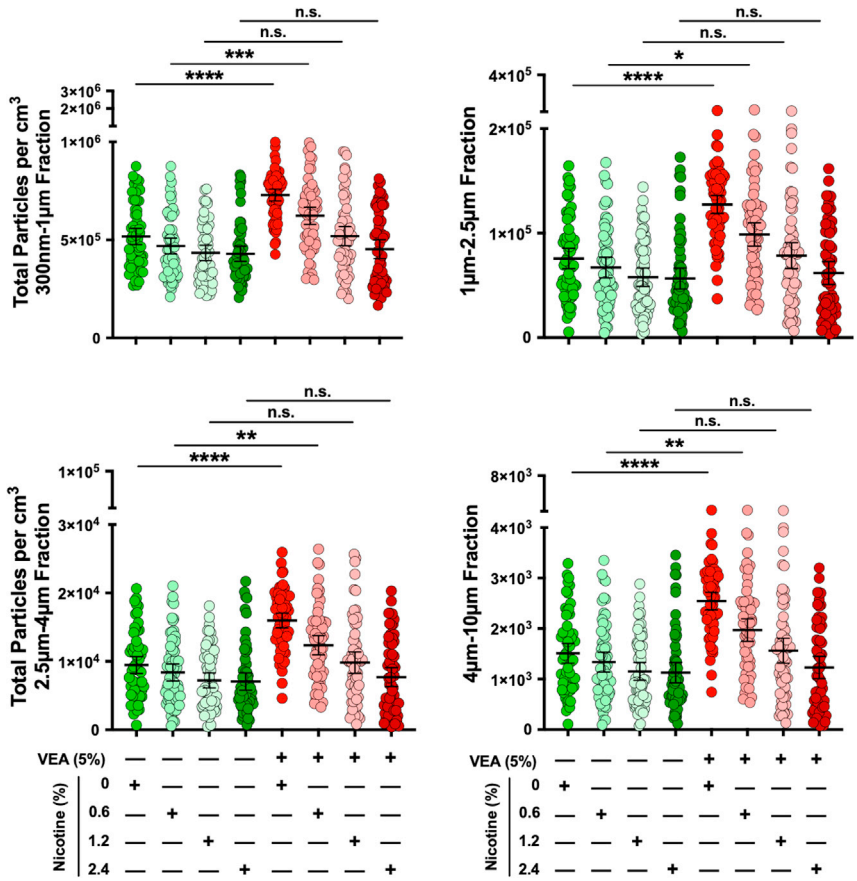

Figure 4. Influence of nicotine alone or in combination with vitamin E acetate on submicron and microparticles generated from electronic cigarette

Distribution profiles of the total particle counts per cm^3 over each inter-puff interval for each size fraction (300 nm–1 µm, 1 µm–2.5 µm, 2.5 µm–4 µm, and 4 µm–10 µm) in the absence or presence of increasing concentration of nicotine (0%, 0.6%, 1.2%, and 2.4% wt/v) with (5% v/v) or without VEA are plotted (all were prepared in 50/50 PG/VG). Kruskal-Wallis test demonstrated statistical significance ($p < 0.0001$). Post-hoc analysis (Dunn's multiple comparison test) showed statistically significant differences between 0% VEA and 5% VEA at both 0% and 0.6% nicotine for all particle size distributions. Error bars indicate mean and 95% confidence intervals for each data set.

Emulating clinically relevant diseased breathing profiles to evaluate impact of VEA on submicron and microparticles in inhaled EC aerosols

In order to better understand the impact that diseased breathing may have on particle distribution dynamics in EC aerosols, we wrote scripts and created software that can actuate the Breathing-Emulator by converting clinical flow-volume loops into breathing profiles. In our studies above, we applied a scaled-down breathing profile of an average healthy human adult. Here, we chose obstructive and restrictive pulmonary disorders (Figure 5A), that encompass COPD, asthma and IPF, as representative lung diseases for breathing profile recapitulation. Unlike our studies in Figures 2, 3, and 4, the experiments here varied the breathing profile, which means that the volumes and inhale/exhale times, and thus volumetric flow rates were different. To normalize for volume and time, the total particles counted per cm^3 were multiplied by the mean flow rate of each breathing profile, and we then plotted the mean total particle flow rate (Figure 5B). We observed that similar to healthy normal breathing, addition of 5% VEA resulted in statistically significant increase in mean total particle flow rate (Figure 5B) and peak concentration (Figure S20) for all four particle fractions in both the obstructive and restrictive breathing profiles. Interestingly, the profile of particle distributions in response to VEA supplementation exhibited a wider range and higher variability with restrictive breathing compared with healthy and obstructive breathings. Moreover, when comparing the differences in mean total particle flow rate for the three breathing profiles at 5% VEA, there was a statistically significant difference from the healthy breathing profile compared with both diseased breathing

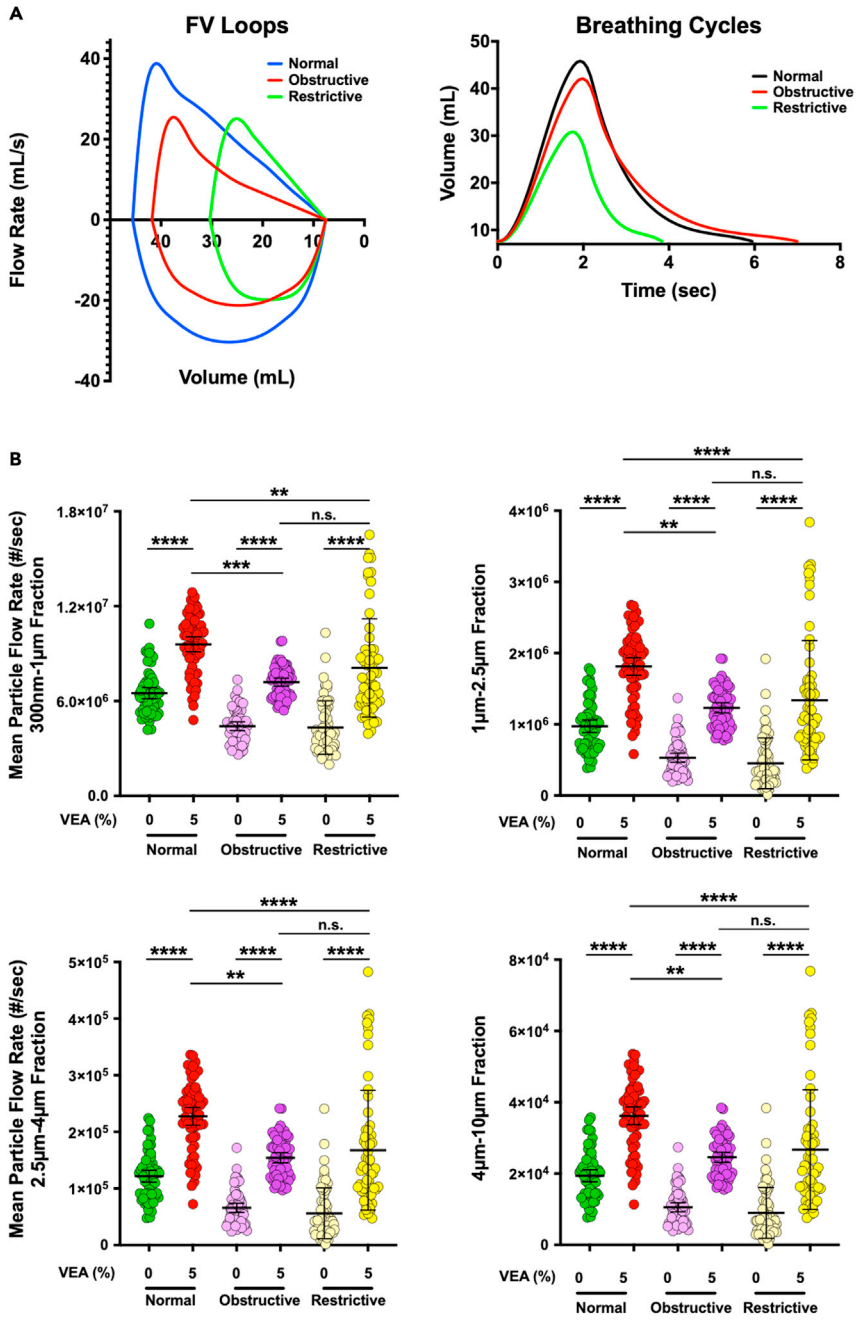

Figure 5. Impact of heathy versus diseased breathing on inhaled mean particle flow rate from electronic cigarette

(A) Healthy (normal) and diseased (obstructive and restrictive) breathing flow-volume loops (left panel) are plotted with normal in blue, obstructive in red, and restrictive in green. The diseased flow-volume loops were derived from clinically relevant scaling and curve changes that are observed by healthy versus obstructive or restrictive breathing profiles. A single breathing cycle for all the breathing states is also plotted (right panel) where volume is a function of time and the graphs are calculating from flow-volume loops.

(B) Distribution profiles of the mean particle flow rate counted per cm^3 over each inter-puff interval for each size fraction (300 nm–1 µm, 1 µm–2.5 µm, 2.5 µm–4 µm, and 4 µm–10 µm) when mimicking healthy normal, obstructive and restrictive breathing in the absence and presence (5% v/v) of VEA in (50/50 PG/VG) are plotted (0% vitamin is just 50/50 PG/VG without any additive). Kruskal-Wallis test demonstrated statistical significance ($p < 0.0001$). Post-hoc analysis (Dunn's multiple comparison test) showed statistically significant differences between all conditions except normal 0% VEA versus both obstructive and restrictive 5% VEA, and obstructive versus restrictive at both 0% and 5% VEA. Error bars indicate mean and 95% confidence intervals for each data set.

profiles. Lastly, we summed the total particles counted per cm^3 over the seven vaping sessions for each breathing profile in the absence or presence of VEA (Figure S21). The cumulative total particle counts were highest with 5% VEA for both normal and obstructive breathing, followed by VEA-containing e-liquid under restrictive breathing. Notably, the magnitude of increase in total particle count due to presence of VEA was highest with the restrictive breathing profile, following sequentially with obstructive and normal breathing.

DISCUSSION

The outbreak of EVALI has caused concern about the respiratory illnesses and deaths associated with the use of ENDSs. Consequently, the FDA and CDC worked closely together and with state and local public health officials to investigate the outbreak. However, very little is known on how inhalation of VEA, which has been suggested as a primary cause of EVALI, leads to lung injury. Historically, the majority of nonclinical studies on vaping have focused on in vitro challenge of lung or immune cells with e-liquid, or exposing animals (most commonly laboratory rodents) to EC aerosols (reviewed by (Merecz-Sadowska et al., 2020)). Yet, lack of physiological relevance (e.g., utilizing cell lines or cancerous cell lines instead of primary well-differentiated cells or tissues), absence of clinically relevant exposure (e.g., submerging cells directly with e-liquid rather than exposing lung cells to EC aerosols under rhythmic breathing, and maintaining natural airway liquid interface seen in conducting airways) and inter-species differences hinder extrapolation of findings from many of these studies of nonclinical models to human. To our knowledge, no peer-reviewed report on impact of VEA-containing EC liquid or aerosols on mucociliated human airway epithelia under air-liquid interface has been published. Importantly, we still do not have a clear picture of how different ingredients and aerosol constituents of ECs such as VEA or nicotine affect the profile and quantity of particles that a human user of ECs actually inhales. This is important information as the higher number of particles generated from an EC can correlate with enhanced deposition in the respiratory tree which can challenge both normal or diseased pulmonary physiology and potentially lead to increased pathological changes and cellular toxicity. In inhalation toxicology, dosimetry of smoke particles has been typically performed using a gravimetric tool (e.g., via quartz crystal microbalances) or an impactor (Adamson et al., 2013; Oldham et al., 2018). However, these are end points, rather than real-time analysis tools. Additionally, variability between and within experiments often affect the interpretation of the data.

Given this critical gap on physical (number and size distribution) characterization of inhaled particles in real-time while emulating breathing and vaping topography and its change in response to modification in EC constituents, we developed the novel system presented here. In addition, to more closely mimic physiological parameters and clinically relevant settings and to provide versatility in utility of the system, we integrated temperature and humidity control along with sensors for precision and correction into our engineered platform. When generating EC aerosols, we recreated physiological breathing, as well as pathological breathing profiles, reproduced vaping topography, included a dilution robot to ensure each freshly generated EC puff mixed well, and diluted into the inspirational tidal volume, and created a software interface to allow users to define each parameter while performing real-time monitoring and collection of the particle size data.

Several industrial smoking/vaping machines that can replicate puff profile have been developed (e.g., by CH Technologies (Kaisar et al., 2017), VitroCell® Systems (Czekala et al., 2019) and Cambustion (Cambustion, 2020)); however, a fundamental drawback of these systems, as well as animal models, is that none of them can emulate and integrate rhythmic human breathing with vaping topography. In addition, some of these platforms lack on-line real-time sensors to characterize particle size distribution and those with sensors do not analyze the highest size values we covered here (that is, 10 μm). Importantly, in our system, we integrated humidifiers and brought the temperature to 37°C to better control for thermodynamic properties and hygroscopic growth of aerosols. It is noteworthy to state that our objective in this study was not to apply our robotic system to predict or mimic EC aerosol behavior within specific branches of lower respiratory tree, such as smaller airways or bronchioles. Rather, we aimed to characterize the profile of EC particles at the site of inspiration (the mouth) just when entering trachea.

We generated RH of 70% inside the exposure Chamber to prevent negative impact on housed electronics and mechanical parts. The RH in oral cavity depends on temperature and RH of input air/gas, and as such varies from individual to individual and in different environments; but in nasopharynx reaches ~100% (Rouadi et al., 1999). We understand that RH is an important factor in aerosol measurement since EC

droplets may change their size due to mass/heat exchange processes as they flow through airways. However, at this point we have developed a unique and proof-of-principle platform that is highly amenable for improvement and user perturbation. In addition, our new approach methodology (NAM) enhances the use of nonclinical testing models for ENDSs to characterize the influence and fate of ingredients in complex mixtures of aerosols. Another notable advantage of the platform is that it is an efficient and reasonable alternative to the ethics, financial cost, and time-consuming reality of animal testing. The FDA encourages use of NAMs using technologies that support the animal 3Rs principals (replace, reduce, refine) to help understand the health risks of all regulated products, including tobacco products (FDA, 2019, 2020). As a future direction, improvements will be made to the insulation sealing around various sensitive components of robotic system so that humidity condensation does not result is shorting circuits, damaging electronics, and rusting mechanical parts. This would enable increasing the RH to 100% (e.g., by increasing the surface area of air-water interface in our embedded humidifiers) allowing us to more accurately take into account the effect of such high RH (which is observed in conducting airways) on particle sizes and predict aerosol deposition within the lungs. Further work can involve simulation to study the effects of flavoring compounds which are known to be appealing to youth (Pepper et al., 2016). Additionally, our system can easily integrate with living tissue models such as Lung Small Airway-on-a-Chip that we previously developed (Benam and Ingber, 2016; Benam et al., 2016a, 2016b, 2017, 2020). As such we plan to evaluate toxicity of different inhaled particle profiles (size and numbers) on mucociliated bronchiolar epithelia in future.

Three major mechanisms influence transport and deposition of aerosols (including EC particles) in human lungs: inertial impaction, gravitational sedimentation, and Brownian diffusion (Darquenne, 2012). When air flow is fast, impaction primarily affects particles larger than 5 μm in size, e.g., as occurs in the upper respiratory tree and at airway bifurcations. Sedimentation on the other hand mostly affects particles in the 1–8 μm range and happens predominantly in small airways and alveoli where the air/aerosol residence time is long and the distance to the lower wall (to be covered by the particles) is short. In contrast, Brownian diffusion is the leading mechanism of deposition for particles $\leq$0.5 μm, and is most relevant in respiratory bronchioles, alveolar ducts, and alveolar cavities – that is acinar region of the lung, where air velocities are very low. Therefore, by specifically evaluating the EC particles in the 300 nm–10 μm range in our studies, we covered the three primary processes that affect their distribution throughout the lungs. Nevertheless, for better insight into ability of generated EC aerosols for Brownian diffusion, an increased capability to quantify and profile nanoparticles (<100 nm in diameter) is required. Our findings notably reveal clues on size-dependent EC particle deposition in the lungs. Approximately 98% of total particles generated from ECs in our studies (Figures 3 and 5), whether VEA and/or nicotine were present in the e-liquid or not, were in the 300 nm–2.5 μm size range. This implies that gravitational sedimentation and Brownian diffusion are the leading drivers for deposition of these particles. In other words, we can deduce that: (1) most EC-derived fresh particles accumulate in the small airways, respiratory bronchioles, alveolar ducts, and alveolar cavities, and thus can impact pulmonary surfactant function; and (2) addition of VEA leads to considerably higher quantities of particle accumulation in these regions of the lung. We need to clarify that these speculations are based on simple PG/VG-containing EC formulations with or without VEA. The addition of reactive aldehydes, phenolic compounds, polycyclic aromatic hydrocarbons, flavorings, and volatile organic compounds to e-liquids may lead to their fast evaporation within oral cavity and hence a different deposition profile.

Recently, Mikheev and colleagues attempted to characterize aerosol size distribution from ECs (Mikheev et al., 2018). However, the sensor used in their studies (a differential mobility spectrometer) (i) lacked high resolution up to 10 μm, (ii) required "sheath flow" in addition to sample flow for measurements, (iii) was not temperature- and humidity-controlled, and (iv) did not couple with a breathing emulator to mimic breathing profile in conjunction with vaping topography. To our knowledge, to date there is no other published study on profiling particle size distribution of ECs containing VEA with or without nicotine in real-time under rhythmic breathing. In addition, our data highlight the importance of focus on injury in alveoli and small airways. For instance, Sosnowski et al., examined physiochemical interactions between EC constituents and lung surfactant (Sosnowski et al., 2018), but the authors used e-liquid in their studies rather than aerosolized submicron and microparticles, and there was no rhythmic breathing (physiological or pathological). Moreover, our findings complement and extend findings from a recent report where authors demonstrated direct negative impact of VEA on mechanical properties of lung surfactant mimics (Dipasquale et al., 2020).

Here, we used a simple PG/VG to study distribution and size profile of inhaled particles in response to increasing representative doses of VEA, nicotine alone or mixed with VEA, and physiological, as well as pathological breathing profiles. Our rationale was that at this stage of technical development, excluding flavoring and a range of proprietary and non-proprietary additive chemicals that various commercial sources include in their e-liquids, can mitigate their impact on our findings. However, in future studies, we can add known EC additives (in a controlled fashion) and investigate their contribution to change in inhaled particle profiles and quantities. Such an approach can be used as a tool to strategically prioritize ingredients and additives in ENDS products for follow-up evaluation of toxicological risks. Likewise, this platform can be useful to identify which ingredients and additives in ENDS products may have a lower impact on inhaled particle profiles and quantities, and thus, lower toxicological concern, which may potentially help reduce the risk from the emissions of ENDS tobacco products. Such information would be informative for protection of public health and from a regulatory science standpoint.

We were intrigued to observe that addition of as little as 1.25% VEA was sufficient to significantly enhance inhaled submicron and microparticles from EC and that the response in particular for the 300 nm–1 μm fraction was augmented as the VEA dose increased to 5%. This may in part explain lung pathology in EVALI as our data show that EC-smokers take in much higher contents of submicron and microparticles in the 300 nm–10 μm range when vaping VEA-supplemented e-liquids. Surprisingly and in contrast, addition of nicotine alone to PG/VG led to reduced, yet non-significant, submicron and microparticle quantities coming from EC. This is consistent with other studies which showed emission of submicron 2.5 μm PM ($PM_{2.5}$) decreases with nicotine (Li et al., 2020). We speculate that this may be attributed to hygroscopic nature of nicotine, which similar to PG/VG, has a low Log Kow (where Kow is n-octanol/water partition coefficient). This is unlike fat-soluble VEA that has a high Log Kow value. A thorough chemical and physical explanation of our observation is beyond the scope of this manuscript. In future, it would be of interest to evaluate impact of tetrahydrocannabinol (THC) – another additive which has been strongly linked to the EVALI outbreak, on particle profile and quantities emitted from ECs and vaping products.

Interestingly, addition of 5% VEA was able to counteract the lowering effect of 0.6% nicotine on submicron and microparticles from EC. Nevertheless, the additive combinatorial impact of VEA did not reach statistical significance in higher doses of nicotine we tested (1.2% and 2.4%). It is important to note that this does not imply it is safe to combine VEA and nicotine at these concentrations. This indicates that additional studies characterizing the ultra-fine particles and gaseous content would provide more information on these interactions; however, these studies are beyond the scope of the current manuscript. Our observation that VEA has a statistically significant effect increasing generated particle quantities and flow rates in all tested fractions and on breathing patterns that emulate both healthy and diseased states is of particular importance. Such enhancing effect is clinically important for obstructive (e.g., COPD or asthma) or restrictive (e.g., IPF) pulmonary disorders. In this study, the disease states were recreated through emulation of breathing flow-volume loops characteristic for the respective disorders. However, pathological changes that would occur due to disease progression disorders, e.g., hypersecretory phenotype, mucus rheology and thickness, goblet cell hyperplasia, reduced lung capacity, could also impact deposition of particles in the respiratory tree.

Prior to selection of PM sensor (Sensirion SPS30) for our studies, we conducted an extensive and exhaustive search on commercially available particle detection systems. We evaluated and compared the Sensirion SPS30 against other light scattering-based optical particle sizers (OPSs) like TSI 3330, personal DataRAM™ pDR-1000AN Monitor, Setra Remote Airborne Particle Counter SPC5000 & SPC7000 Series, Aeroqual AQM 65 Ambient Air Monitoring Station, Atmotube Pro, Palas Promo® LED 2300, and Malvern Panalytical Mastersizer 3000, aerodynamic particle sizers (APS, which use the principle of inertia to size particles) like TSI 3321, scanning mobility particle sizer (SMPS) spectrometers (which are based on the physical principle that the ability of a particle to pass through an electric field – i.e., its electrical mobility, is fundamentally related to its size; these detectors use condensation particle counters [CPC] for sensing) like TSI 3938, and fast mobility particle sizer (FMPS) spectrometers (which use an electrical mobility measurement technique similar SMPS systems, but instead of CPC they utilize multiple, low-noise electrometers for particle detection) like TSI 3091. We found that these sensors, unlike the Sensirion SPS30, have one or more of these drawbacks rendering them incompatible for our platform: (1) requiring a pump that is controlled by sensor, whereas we needed to retain the ability to control the flow rate as it is dynamic and low; (2) requiring high

flow rates (often in multiples of L/min) to allow particle detection, while we needed lower flow rates (~360 mL/min for 30 mL stroke volumes); (3) incompatibility for real-time sensing and analysis; (4) having large dead volumes; (5) requiring a slow sampling rate; (6) needing to heat up the input gas to high temperatures before analyzing; (7) incompatibility with environmental humidity and temperature set points that we needed for our studies; (8) being too large and designed as standalone benchtop systems that could not fit within a compact and user-controllable system like our inhalation exposure chamber; (9) inability to integrate with (micro)fluidic connections – e.g., some sensors have been developed for ambient air/gas conditions and do not offer ability to control flow; (10) requiring a sheath gas to be passed along with the sampled air/gas; and (11) inability to detect the wide particle size ranges we investigated here. As such, despite the fact that few of these sensors had the ability to quantify particles <300 nm, we were unable to integrate them with our platform for real-time nanoparticle detection while mimicking breathing profile and vaping topography at desired temperature, humidity, and flow rate. Such limitations hindered us from studying ultra-fine particles in this study. However, in follow-up studies we will explore modifications to existing nanoparticle sensors and/or development of a new nanosensor (most likely SMPS- or FMPS-based) for incorporation into our system.

In summary, here we report development and application of a robust, and physiologically and clinically relevant engineered system to evaluate submicron and microparticles generated from any desired EC (filled with constituents of interest) in real-time. Utilizing this platform, we observed that addition of VEA to e-liquid leads to significantly higher quantities of particles from EC, which may in part explain some of the lung pathologies observed in EVALI. Importantly, this impact of VEA was evident even when emulating the breathing profiles of obstructive and restrictive lung disorders. As a research proof-of-principle tool, this platform is powerful because it provides exposure information on ingredients and additives emitted from ENDS products to facilitate the health risk evaluation of ENDS products. As the next step, we believe it is key to enhance the capabilities of our platform to allow studying ultra-fine particle smaller than 300 nm in parallel with 300 nm–10 μm range that we examined here, investigate the influence of THC, and mechanistically dissect chemical and physical properties of e-liquid additives in PG/VG mixture that lead to such differential particle profiles and quantities.

Limitations of the study

This study is the starting point for a quantitative bio-inspired analysis into inhaled particle profiles from ENDSs for toxicological evaluation. Ability to detect ultrafine particles smaller than 300 nm and recreate humidity levels above 70% (if/when needed) would further strengthen our robotic system.

STAR★METHODS

Detailed methods are provided in the online version of this paper and include the following:

- KEY RESOURCES TABLE
- RESOURCE AVAILABILITY
  - Lead contact
  - Materials availability
  - Data and code availability
- METHOD DETAILS
  - Vaping robot
  - Dilution robot
  - Real-time particle detection system
  - Breathing-emulator
  - Inhalation exposure chamber
  - Programming and coding
  - Data processing
  - Real-time quantitative analysis of EC aerosols
- QUANTIFICATION AND STATISTICAL ANALYSIS

SUPPLEMENTAL INFORMATION

Supplemental information can be found online at https://doi.org/10.1016/j.isci.2021.103091.

ACKNOWLEDGMENTS

We thank CU Denver Inworks and Dr. Richard Weir for their help with 3D printing and laser cutting several parts used in out platform. This work was supported by the Division of Pulmonary, Allergy and Critical Care Medicine at University of Pittsburgh, the U.S. Food and Drug Administration (HHSF223201810127C), the U.S. National Institutes of Health (U01EB029085; R41ES031639), and the U.S. Department of Defense Congressionally Directed Medical Research Programs Discovery Award (W81XWH2010035). L.G.V.: The findings and conclusions in this report are those of the authors and do not necessarily represent the official position of the U.S. Food and Drug Administration, U.S. Department of Defense or the U.S. government.

AUTHOR CONTRIBUTIONS

K.H.B. and A.J.K. designed the research; A.J.K. and C.S. designed the vaping robot; A.J.K., C.S., and B.J.A. fabricated the vaping robot, designed and fabricated the inhalation exposure chamber, and designed and fabricated the particulate matter sensor gasket system; A.J.K. designed and fabricated the dilution robot, as well as designed and fabricated the breathing-emulator; A.J.K., B.J.A., K.P.S., and A.P. developed the code to assist in processing the data; A.J.K. and A.P. collected and analyzed the data; A.J.K., C.S., B.J.A., K.P.S., and A.P. prepared the manuscript; and L.G.V. and K.H.B. critically revised the manuscript.

DECLARATION OF INTERESTS

K.H.B. is founder and holds equity in Pneumax, LLC. K.H.B. is in a co-inventor on patent applications related to technologies presented here.

Received: May 28, 2021
Revised: July 29, 2021
Accepted: September 1, 2021
Published: September 29, 2021

REFERENCES

20768:2018, ISO (2018). Vapour Products — Routine Analytical Vaping Machine — Definitions and Standard Conditions [Online]. https://www.iso.org/standard/69019.html.

Adamson, J., Thorne, D., Mcaughey, J., Dillon, D., and Meredith, C. (2013). Quantification of cigarette smoke particle deposition in vitro using a triplicate quartz crystal microbalance exposure chamber. Biomed. Res. Int. *2013*, 685074.

Benam, K.H., and Ingber, D.E. (2016). Commendation for exposing key advantage of organ chip approach. Cell Syst. *3*, 411.

Benam, K.H., Novak, R., Nawroth, J., Hirano-Kobayashi, M., Ferrante, T.C., Choe, Y., Prantil-Baun, R., Weaver, J.C., Bahinski, A., Parker, K.K., and Ingber, D.E. (2016a). Matched-comparative modeling of normal and diseased human airway responses using a microengineered breathing lung chip. Cell Syst. *3*, 456–466 e4.

Benam, K.H., Villenave, R., Lucchesi, C., Varone, A., Hubeau, C., Lee, H.H., Alves, S.E., Salmon, M., Ferrante, T.C., Weaver, J.C., et al. (2016b). Small airway-on-a-chip enables analysis of human lung inflammation and drug responses in vitro. Nat. Methods *13*, 151–157.

Benam, K.H., Mazur, M., Choe, Y., Ferrante, T.C., Novak, R., and Ingber, D.E. (2017). Human lung small airway-on-a-chip protocol. Methods Mol. Biol. *1612*, 345–365.

Benam, K.H., Novak, R., Ferrante, T.C., Choe, Y., and Ingber, D.E. (2020). Biomimetic smoking robot for in vitro inhalation exposure compatible with microfluidic organ chips. Nat. Protoc. *15*, 183–206.

Bhat, T.A., Kalathil, S.G., Bogner, P.N., Blount, B.C., Goniewicz, M.L., and Thanavala, Y.M. (2020). An animal model of inhaled vitamin E acetate and EVALI-like lung injury. N. Engl. J. Med. *382*, 1175–1177.

Blount, B.C., Karwowski, M.P., Shields, P.G., Morel-Espinosa, M., Valentin-Blasini, L., Gardner, M., Braselton, M., Brosius, C.R., Caron, K.T., Chambers, D., et al. (2020). Vitamin E acetate in bronchoalveolar-lavage fluid associated with EVALI. N. Engl. J. Med. *382*, 697–705.

Bowler, R.P., Hansel, N.N., Jacobson, S., Graham Barr, R., Make, B.J., Han, M.K., O'Neal, W.K., Oelsner, E.C., Casaburi, R., Barjaktarevic, I., et al. (2017). Electronic cigarette use in US adults at risk for or with COPD: analysis from two observational cohorts. J. Gen. Intern. Med. *32*, 1315–1322.

Cambustion. (2020). SCS Smoking/Vaping Machine [Online]. https://www.cambustion.com/products/scs.

Czekala, L., Simms, L., Stevenson, M., Tschierske, N., Maione, A.G., and Walele, T. (2019). Toxicological comparison of cigarette smoke and e-cigarette aerosol using a 3D in vitro human respiratory model. Regul. Toxicol. Pharmacol. *103*, 314–324.

Darquenne, C. (2012). Aerosol deposition in health and disease. J. Aerosol Med. Pulm. Drug Deliv. *25*, 140–147.

Dipasquale, M., Gbadamosi, O., Nguyen, M.H.L., Castillo, S.R., Rickeard, B.W., Kelley, E.G., Nagao, M., and Marquardt, D. (2020). A mechanical mechanism for vitamin E acetate in E-cigarette/vaping-associated lung injury. Chem. Res. Toxicol. *33*, 2432–2440.

Duffy, B., Li, L., Lu, S., Durocher, L., Dittmar, M., Delaney-Baldwin, E., Panawennage, D., Lemaster, D., Navarette, K., and Spink, D. (2020). Analysis of cannabinoid-containing fluids in illicit vaping cartridges recovered from pulmonary injury patients: identification of vitamin E acetate as a major diluent. Toxics *8*, 8.

FDA (2019). Premarket Tobacco Product Applications for Electronic Nicotine Delivery Systems - Guidance for Industry [Online]. https://www.fda.gov/media/127853/download.

FDA (2020). FDA's Predictive Toxicology Roadmap [Online]. https://www.fda.gov/science-research/about-science-research-fda/fdas-predictive-toxicology-roadmap.

Kaisar, M.A., Villalba, H., Prasad, S., Liles, T., Sifat, A.E., Sajja, R.K., Abbruscato, T.J., and Cucullo, L. (2017). Offsetting the impact of smoking and e-cigarette vaping on the cerebrovascular system and stroke injury: is metformin a viable countermeasure? Redox Biol. *13*, 353–362.

Kozlovich, S., Harvanko, A.M., and Benowitz, N.L. (2021). Vitamin E acetate is not soluble in nicotine E-liquids. Tob. Regul. Sci. *7*, 130–134.

Krishnasamy, V.P., Hallowell, B.D., Ko, J.Y., Board, A., Hartnett, K.P., Salvatore, P.P., Danielson, M., Kite-Powell, A., Twentyman, E., and Kim, L. (2020).

Update: characteristics of a nationwide outbreak of E-cigarette, or vaping, product use-associated lung injury - United States, August 2019–January 2020. Morb. Mortal. Wkly. Rep. *69*, 90–94.

Li, L., Lee, E.S., Nguyen, C., and Zhu, Y. (2020). Effects of propylene glycol, vegetable glycerin, and nicotine on emissions and dynamics of electronic cigarette aerosols. Aerosol Sci. Technol. *54*, 1–12.

Merecz-Sadowska, A., Sitarek, P., Zielinska-Bliźniewska, H., Malinowska, K., Zajdel, K., Zakonnik, L., and Zajdel, R. (2020). A summary of in vitro and in vivo studies evaluating the impact of E-cigarette exposure on living organisms and the environment. Int. J. Mol. Sci. *21*, 652.

Mikheev, V.B., Ivanov, A., Lucas, E.A., South, P.L., Colijn, H.O., and Clark, P.I. (2018). Aerosol size distribution measurement of electronic cigarette emissions using combined differential mobility and inertial impaction methods: smoking machine and puff topography influence. Aerosol Sci. Technol. *52*, 1233–1248.

Muthumalage, T., Lucas, J.H., Wang, Q., Lamb, T., Mcgraw, M.D., and Rahman, I. (2020). Pulmonary toxicity and inflammatory response of E-cigarette vape cartridges containing medium-chain triglycerides oil and vitamin E acetate: implications in the pathogenesis of EVALI. Toxics *8*, 46.

Oldham, M.J., Zhang, J., Rusyniak, M.J., Kane, D.B., and Gardner, W.P. (2018). Particle size distribution of selected electronic nicotine delivery system products. Food Chem. Toxicol. *113*, 236–240.

Overbeek, D.L., Kass, A.P., Chiel, L.E., Boyer, E.W., and Casey, A.M.H. (2020). A review of toxic effects of electronic cigarettes/vaping in adolescents and young adults. Crit. Rev. Toxicol. *50*, 1–8.

Pepper, J.K., Ribisl, K.M., and Brewer, N.T. (2016). Adolescents' interest in trying flavoured e-cigarettes. Tob. Control *25*, ii62–ii66.

Reagan-Steiner, S., Gary, J., Matkovic, E., Ritter, J.M., Shieh, W.J., Martines, R.B., Werner, A.K., Lynfield, R., Holzbauer, S., and Bullock, H. (2020). Pathological findings in suspected cases of e-cigarette, or vaping, product use-associated lung injury (EVALI): a case series. Lancet Respir. Med. *8*, 1219–1232.

Rouadi, P., Baroody, F.M., Abbott, D., Naureckas, E., Solway, J., and Naclerio, R.M. (1999). A technique to measure the ability of the human nose to warm and humidify air. J. Appl. Physiol. *87*, 400–406.

Sosnowski, T.R., Jablczynska, K., Odziomek, M., Schlage, W.K., and Kuczaj, A.K. (2018). Physicochemical studies of direct interactions between lung surfactant and components of electronic cigarettes liquid mixtures. Inhal. Toxicol. *30*, 159–168.

Wu, D., and O'Shea, D.F. (2020). Potential for release of pulmonary toxic ketene from vaping pyrolysis of vitamin E acetate. Proc. Natl. Acad. Sci. U. S. A. *117*, 6349–6355.

STAR★METHODS

KEY RESOURCES TABLE

REAGENT or RESOURCE	SOURCE	IDENTIFIER
Chemicals, peptides, and recombinant proteins		
(+/−)-A-Tocopherol Acetate	Sigma-Aldrich	T3376-100G
Propylene Glycol	Sigma-Aldrich	W294004-1KG-K
Glycerol	Sigma-Aldrich	W252506-1KG-K
Software and algorithms		
Custom SPS30 sensor processing software	This article	Available from lead contact upon request

RESOURCE AVAILABILITY

Lead contact

Further information and requests for resources and reagents should be directed to and will be fulfilled by contacting Kambez H. Benam (benamk@pitt.edu).

Materials availability

This study did not generate new unique reagents.

Data and code availability

The data that support the findings of this study, the code for analysis and any additional information are available from the corresponding author upon reasonable request.

METHOD DETAILS

Vaping robot

The aerosols exposure system was designed to be physiologically analogous to a human using ENDS products. The production of aerosols is accomplished by a small, enclosed robot, referred to as the Vaping Robot, that can emulate any human 'vaping profile'. The robot generates a negative pressure with a small internal pump that is strong enough to trigger the aerosolization of the liquid in the electronic vaping cartridge. The aerosols are then directed through a series of small pneumatic pinch-valves, where the aerosols can be sampled into the Inline Particulate Matter (PM) Sensor at the specified time and the specified intervals.

The EC is sealed with a polydimethylsiloxane (PDMS) gasket, which was molded to fit into a hollow nut and bolt custom designed and 3D printed with VeroClear™. This allows for quick and cheap production of disposable interchangeable mouthpieces for testing different styles of electronic aerosolization devices if desired. The mouth is imitated with a 55 mL polypropylene pneumatic syringe reservoir that is just upstream of the vacuum pump. The pump itself simulates the vacuum generated in the mouth which triggers the aerosol production from the electronic smoking device. The Breathing-Emulator will constantly be taking breaths through the PM Sensor and filters within the Vaping Robot but can also sample the aerosols with the same breathing profile at the puff intervals specified.

The robot itself has an acrylic housing with two sliding doors for maintenance and loading access. There are two internal chambers to isolate and protect the electronic equipment from copious amounts of ambient aerosols or smoke. Shelving and 3D printed parts help organize the pneumatic components and allow the aerosols to flow in a downhill direction to avoid goosenecks in the tubing and to prevent re-condensation on the surface and potential clogs. The system consists of four pinch valves and a vacuum where the pinch valves allow for fluidic connections of the Dilution Robot and PM Sensor, which is also connected to the Breathing-Emulator. Specifically, the reservoir within the Dilution Robot is connected to either the ambient air or the EC, as well as fluidic connections on the other side of the reservoir to the vacuum pump or the Breathing-Emulator. Additionally, there are fluidic connections for the Breathing-Emulator to the reservoir or to the inhale or exhale filters.

An Arduino Uno microcontroller and an 8-channel relay shield, which is controlled by the microcontroller through an I2C communication protocol, were used to control the timing of the pneumatic pinch-valve configuration and vacuum pump activation. This is accomplished by opening and closing the appropriate fluidic paths so that the aerosols or air can travel into the intended components. The vacuum pump was controlled by a higher amperage relay that was in turn controlled by a channel on the shield; the pinch valves were controlled directly by a channel on the shield.

The Vaping Robot has multiple states that when combined have two main sequences, one for vaping and one for filtered air breathing. For the vaping sequence, the pinch valves start fluidically disconnecting the Breathing-Emulator from the reservoir and are instead connected to the inhale and exhale filters. A direct path for aerosols is opened from the pump to the reservoir and from the reservoir to the EC. The pump is then activated in accordance with the vaping profile of choice, and the aerosol generated from the EC is collected in the reservoir. Once the aerosol is collected and after the specified dilution has occurred from the Dilution Robot, the pinch valves fluidically connect the Breathing-Emulator to the reservoir, allowing for a breath that samples the aerosols to occur. After the Breathing-Emulator has sampled the aerosols into the PM Sensor, the reservoir is cleared with the vacuum pump, similar to how the EC is activated except the reservoir is connected to the external air. For the filtered air breathing sequence, the pinch valves are configured similarly to the beginning of the vaping sequence where the Breathing-Emulator is fluidically connected to the inhale and exhale filters. Specifically, the Breathing-Emulator's fluidic connection with the inhale and exhale filters are toggled in synchrony with the Breathing-Emulators inhale/exhale state. Since the Breathing-Emulator generates both positive and negative pressure within the tubing, the sampling sequence was designed to account for this fluctuation and open pinch valves that would relieve negative pressure buildup without allowing for the aerosols sample to be expelled from the system in addition to preventing the aerosols sampled from re-entering the reservoir.

Dilution robot

The Dilution Robot was designed to dilute aerosols within the reservoir before analyzing the aerosols with the PM Detection System. This is accomplished by mixing a calculated volume of filtered air with the reservoir and potentially removing a fraction of the mixed aerosols and re-diluting before the aerosols is sampled into the PM Sensor. The system was designed to allow for the user to control the level of particle delivered to the PM Sensor or other systems such as lung-on-a-chip devices to mimic physiologically relevant parameters by including dilutions that would be seen in the lungs through the mixing of the tidal volume and the dead space. Dilution can also be used if there are saturation limits within one of the systems. The Dilution Robot theoretically has no lower dilution limit, but the dilution time is dependent on the dilution ratio.

The Dilution Robot operates through pumping fresh air into the reservoir with a 30 mL syringe, referred to as the Sample syringe. The excess volume is captured in another 30 mL syringe referred to as the mixing syringe. The system then, if required to dilute further, will sample a calculated number of diluted aerosols in the reservoir. The reservoir will then be cleared with the vacuum pump and the aerosols in the sample syringe are injected into the reservoir for further dilution. If further dilution is needed, this process can be repeated. The process is initiated by a signal from the Vaping Robot indicating that the reservoir is filled with aerosol. After the Dilution Robot has finished the dilution, it will enter a standby phase, referred to as VR Connect, waiting for the Vaping Robot to sample the aerosols, where it will enter the PM Sensor. Once the sampling is complete, a signal is sent from the Vaping Robot to the Dilution Robot indicating that the system can start preparing for the next aerosols puff. After this signal is sent either the Vaping Robot or the Dilution Robot will clear the reservoir, depending on the configuration, the Dilution Robot will then enter VR Connect waiting for the next aerosols puff.

The Dilution Robot has an acrylic frame that supports all the components and mounts on top of the Vaping Robot. There are access holes on the bottom of the Dilution Robot so that the connections on the Vaping Robot can be connected to the reservoir within the Dilution Robot. There are two main chambers within the Dilution Robot, the top chamber contains the linear servo motor which drives the syringe actuation adapter. This adapter actuates two plungers that are each connected to syringes pointed in opposite directions. The design allows for conservation of volume while being able to move aerosols/air into sections that can then be fluidically disconnected through the pinch valve array. The pinch valve array is contained in the bottom chamber along with the vacuum pump, filters, and electronics. The pinch valve arrays are

connected so that air can be taken in or expelled through different filters from the sample syringe. The mixing syringe can intake from the reservoir and expel through another filter. The reservoir can be connected to the two syringes, sample and mixing, to the Vaping Robot, or to a larger filter and the vacuum pump.

The Dilution Robot is controlled with an Arduino Uno connected to the same type of 8 channel relay shield used in the Vaping Robot. Similarly, the Dilution Robot's pinch valves and vacuum are triggered by activating relays which are commanded through the I2C interface. Additionally, a servo motor controller (Actuonix Linear Actuation Control Board) receives commands through a PWM signal generated from the firmware, the servo controller then drives that linear servo (Actuonix, Cat. #: P16-100-64-12-P).

Real-time particle detection system

To detect the real-time levels of particle sizes being produced by the e-cigarette aerosols, a PM Sensor needed to be incorporated into the system. The PM Sensor selected was the Sensirion SPS30, which allowed for the detection of particles ranging from 300 nm to 10 μm and provided particle count and mass concentration readings. The PM Sensor uses an optical detection design, where as a particle travels through the PM Sensor housing, it reaches a laser that is constantly active. As a particle traverses through the laser, light is scattered and then reaches a photodiode, which then sends a signal to a processing unit which determines the size of the particle based on factors such as amount of scattered light detected.

A custom-built enclosure for this PM Sensor needed to be designed in order to allow for a PM Sensor to be able to receive aerosol samples. This enclosure primarily consisted of a two-piece mold-cast PDMS gasket, which provided an airtight seal around the PM Sensor itself and isolated the inlet and outlet ports from one another to be able to achieve directional flow for the aerosol samples within the overall testing system. The PDMS gasket allowed for respective inlet and outlet tubing posts to be embedded so the PM Sensor could interface with the rest of the tubing in the testing system. To provide compression to the two-piece gasket to further ensure an airtight seal, a support frame consisting acrylic plating, was fabricated. This PM Sensor enclosure was placed in-line with the Vaping Robot and the Breathing-Emulator; hence the input port receives the aerosols from the Robot, and the sample is driven through the PM Sensor and output port via the Breathing-Emulator.

To operate the PM Sensor and retrieve data in real time, a circuit board was designed in order to power the PM Sensor and connect it to a microcontroller. Firmware was written to receive and store the data transmitted while the PM Sensor is active. When the full system is powered on, the PM Sensor is activated and starts collecting data for the full duration of the aerosols collection trial. The data can be monitored via the data log or a graphical user interface that was developed in order to immediately plot the data in a graph sectioned by particle size ranges of 300 nm – 1 μm, 1 μm – 2.5 μm, 2.5 μm – 4 μm, and 4 μm – 10 μm, for real-time visual interpretation of the current aerosols analyzed. For the comparison of all trials collected, the data was processed afterwards using MATLAB and GraphPad Prism, which is further detailed in the Data Processing section.

Breathing-emulator

The Breathing-Emulator was designed to emulate the dynamic nature of volume displacement within the lungs during either inhalation or exhalation. The software actuating the Breathing-Emulator translates a selected flow-volume loop and converts this into a cyclic series of volume displacement values and volume displacement rates. This segmented data corresponds to many small, linear in velocity, seeks which when concatenated gives a dynamic breathing curve. The syringe plunger is then actuated to displace the volume of air within the syringe at the programmed rate, where the nozzle of the syringe can be connected to other systems.

The mechanical design of the Breathing-Emulator achieves three major goals: maintaining reliable long-term operation, stable operation in biological incubator environments, and dynamic displacement of air through executing user specified breathing patterns. To dynamically displace air with a syringe, the velocity of the plunger being actuated must also be dynamic. The design has an acrylic based frame, that mounts a motor, which drives a carriage that actuates the plungers through a nut and lead screw system. This allows the motor to be programmed with a complex step rate and step profile to give dynamic, user specified, actuation.

Reliability of the system is also highly important, especially when many or long experiments are being performed. Conventional stepper motors do not have positional feedback and are an open loop system. Over time motor steps are occasionally skipped resulting in drift of the carriage and the plunger used to displace the volume of air. The Breathing-Emulator was designed to have one large motor instead of multiple smaller motors. Using multiple smaller motors to drive the carriage could lead to the steps becoming desynced between the motors, causing misalignment in the system, torque on the plunger against the syringe walls and damage to components. However, since the system is being driven by a single motor, the motor needs to be capable of supplying sufficient power to move the carriage and syringe plungers; if not, the inability to meet torque required could result in many skipped steps. An additional reliability design feature was adding endstops, or limit switches, to the stroke limits of the system. The endstops will be mechanically trigged and inform the program to correct for the drift and resume operation if enough steps have been skipped that a non-negligible drift has occurred.

The motor is the primary electro-mechanical component on the Breathing-Emulator. Since standard motors can be damaged from high humidity and requires adequate thermal dissipations and the incubators are set to high humidity levels and temperatures above ambient air, we selected a high-power, humidity proof, stepper motor for the design. With the specified stepper motor, acrylic frame, and minimal metal parts, the system can operate long term with environments that are in an incubator.

The mechanical design, as mentioned, is an acrylic frame with a stepper motor mounted that rotates a lead screw, which actuates the carriage through a nut in the center of the carriage. On the other side of the lead screw is an idler that allows for free rotation of the lead screw. On each side of the carriage is a set of linear bearings that slide along a guide rail to prevent the carriage from rotating when the nut is rotated, thus allowing the rotational movement to be translated into linear movement. Additionally, the guide rails allow for accurate axis straightness during actuation. All components other than the motor are mounted to adapters; this allows for components to be swapped out without redesigning the Breathing-Emulator. Both the syringes and plungers experience axial force during actuation. To prevent movement of the syringes as well as displacement changes of the plunger relative to the carriage, caps are added to the adapters. The caps are bolted to the adapters to pin the components; the syringe has a single cap on the top and the plunger has a cap on the top and bottom. On one side of the frame is two ports for inserting endstops, and the corresponding adapters. Each endstop is on opposite sides of the seek limits of the carriage. The endstop closest to the syringes are used for both homing the Breathing-Emulator and detecting lower bound seek errors. The other endstop, closest to the motor, is responsible for detecting upper bound seek errors.

A peripheral printed circuit board (PCB) was designed to control the Breathing-Emulator motor. The PCB is a shield, meaning that it plugs into another electronic controller, in this case an Arduino Uno. The Arduino Uno runs the Breathing-Emulator firmware which communicates with the motor driver on the PCB. The motor driver is controlled through 5 main pins: step, direction, micro-step 1, micro-step 2, and micro-step 3. Every time an electrical 5V pulse is sent to the step pin, the motor driver commands the motor to take a step. In this configuration, a whole step is $1/200^{th}$ of a rotation, but the steps can also be configured to be fractions of a step by multiples of 2, such as half step, quarter step, 1/8th step, and 1/16th step. These fractional steps, called micro-steps, can be configured through setting the 3 micro-step pins. The direction pin controls the direction that the motor rotates and is dependent on a 5V or 0V signal. The motor driver also contains a few unused pins and power related pins, VDD the motor driver power pin, VMOT the motor power pin, and GND the ground pins. The motor driver also has 4 stepper motor driver pins, these pins connect to a 2-phase stepper motor to deliver the required power profile to the motor.

The PCB, along with the stepper motor driver contains header pins to connect afferent and efferent connections to the PCB. These headers include four 2-pin afferent connections for the 12V power that is used to power both the motor and the Arduino Uno, the inhale/exhale signal that is used to synchronize the Vaping Robot with the Breathing-Emulator, and the two endstop headers used to detect if the endstops were triggered. Additionally, there is one efferent 4-pin header for the 2-phase motor. The PCB also contains two electrical filters, which reduce the noise observed by the Arduino Uno during the voltage transition of the endstop, which is triggered by the switch being mechanically depressed. The PCB includes a green light emitting diode to indicate when running and a button that can be toggled to turn the system on and off.

The firmware is executed by the Arduino and controls operation of the Breathing-Emulator. The foundation of the firmware configures the Arduino hardware to generate a dynamic series of pulses to control the motors rotation by setting hardware registers that configure the internal timers which periodically invoke custom interrupt service routines. When the firmware reads a delay value for the motor pulses, it calculates the clock frequency and updates the hardware timers. When the timers invoke the service interrupt routine a step is issued the next delay and step count is indexed, this process is on a continuous loop.

Inhalation exposure chamber

The Inhalation Exposure Chamber (outer dimensions: 710 mm x 560 mm x 650 mm) was designed under the premise of conducting the entirety of the aerosol inhalation trials in an environment that resembles the human lung, in order to provide data which is more physiologically relevant. The chamber was designed to provide a workspace to house the Breathing-Emulator, Vaping Robot, and the PM Detection System, while generating an internal environment that maintains stable temperature, humidity, and carbon dioxide (CO_2) levels at 5% (commonly used in laboratory tissue culture incubators, enabling use of our system in future for *in vitro* exposure studies), and allows for the ejection of accumulated aerosols buildup. The chamber consists of an environmental control system, and a vacuum ejection system. The environmental control system consists of three subsystems: temperature regulation, humidity regulation, and CO_2 regulation. The chamber utilizes a microcontroller with a custom-designed PCB and custom firmware that was designed and written to provide simultaneous regulation of the environmental control subsystems and vacuum ejection system. A key point in the chamber design was for it to be self-regulating and function automatically without user intervention. To accomplish this, the subsystems of the environmental control system utilize a PID (proportional-integral-derivative) algorithm with feedback mechanisms to account for any changes to the internal environment of the chamber and to maintain a stable setpoint. This is important for aerosols collection trials, where the chamber maybe repeatedly opened to swap e-cigarette cartridges or perform maintenance to any of the other systems within the Inhalation Exposure Chamber.

The temperature regulation subsystem consists of an array of digital thermometer sensors positioned along the inner walls of the chamber to obtain an accurate depiction of internal temperature, as well as a set of heater units. The heater units have independently controlled fans and are fitted on angled mounts, with opposite directions of flow in order to promote proper convection. The sensors relay information back to the central microcontroller and the subsystem firmware detects if the internal temperature is at the setpoint defined (in our case 37°C). If the temperature is below the setpoint, the heater units are active until the setpoint temperature is reached. As the internal temperature approaches the setpoint, the intensity of the heater units is automatically reduced to avoid thermal overshoot. Once the setpoint is reached, the heaters stably maintain the temperature within ± 0.5°C. This algorithm allows the subsystem to respond immediately to changes in the internal environment, such as opening the chamber or if removal of internal air with the purge functionality; the heater fan intensity can increase or decrease accordingly to stabilize the internal temperature towards the setpoint.

The CO_2 regulation subsystem was designed in a similar manner. A sensor measures internal CO_2 levels and sends this information to the central microcontroller, which then calculates the amount of CO_2 that needs to be injected into the chamber. This subsystem consists of the CO_2 sensor, two pneumatic pressure regulators, an injection tank of known volume, and series of pneumatic solenoids to control the flow of CO_2 gas. The microcontroller determines the amount of CO_2 to be injected using a PID algorithm which determines the pressure levels needed to reach the defined setpoint of 5% CO_2, as well as the frequency that injections need to be introduced into the chamber. This allows for increasing the CO_2 levels within the chamber to reach and maintain the setpoint while avoiding overshooting the amount of CO_2 introduced. The frequency and amount of CO_2 injected is reduced as the internal levels reach that of the setpoint. If a dramatic overshoot is detected, a second pressure regulator is activated in order to allow for the injection of clean air into the chamber to reduce the CO_2 concentration.

The humidity regulation subsystem was designed similarly to the temperature regulation subsystem, utilizing a RH sensor to provide information to the central microcontroller about the internal humidity of the chamber. This subsystem was mainly designed so this chamber platform could be used to perform aerosols exposure trials on live cells. If the RH was detected below the defined setpoint of 70%, then a humidifier unit would be activated to reach and maintain the humidity setpoint. This humidifier unit was designed with a small footprint, a lid with perforated holes that allows for humidity to escape the unit while reducing larger

droplets from exiting the chamber as well as transparent housing that allows for monitoring of current water levels.

This environmental control system allowed for all trials to be conducted at 37°C, 70% RH, and 5% CO_2 concentration. The code for all the subsystems within the Inhalation Exposure Chamber is combined into a singular controller firmware for simultaneous regulation of each process, while also allowing for controlling the vacuum ejection system. The vacuum ejection system is a binary system and was designed to remove any particle build up that occurs during the aerosols trials or other experiments. This system consists of a series of solenoids, filters, and a high flow rate vacuum pump. The solenoids are normally closed to maintain an isolated internal environment. When activated, the solenoids impeding flow from the chamber to the vacuum pump are opened and the pump is activated. A solenoid impeding flow from the chamber to open air is also opened simultaneously to allow air into the chamber. All air being removed and introduced passes through inline HEPA filters, and the system was designed in order to equilibrate pressure while it is activated, so there is no negative pressure buildup internally. The vacuum ejection system is manually triggered when the user determines that there is sufficient smoke buildup using a dedicated GUI control program designed for the Inhalation Exposure Chamber; alternatively, the system can be set to activate on a timer.

The Inhalation Exposure Chamber consists of a metal bracket frame, providing most of the support structure for the chamber, and double-paned acrylic panels for the walls. This allows for a proper sealed insulation of heat, humidity, and gas within the chamber to maintain the setpoints and provide an isolated internal environment. Within the chamber is a custom humidifier unit and a set of support rails along the wall panels that allow for the placement of necessary internal electronic components, such as heaters, fans, sensors, and isolated wiring. On the back side of the chamber, separated from the main internal chamber, is an electronics component compartment which houses the majority of the electrical components of the Inhalation Exposure Chamber, including the microcontroller that drives all functions of the chamber, as well as the mounted custom PCB. This PCB contains the circuitry for all the systems and their connection to the microcontroller. This compartment also houses other electronic components such as relays, converters, and power supply units. All pneumatic components for the chamber, except for the externally connected vacuum pump and associated solenoid, also reside in this compartment, such as pressure regulators, tanks, tubing, solenoids, and air filters.

Programming and coding

The various subsystems of the project required programming to function, including: The Vaping Robot, PM Detection System, Inhalation Exposure Chamber, Breathing-Emulator, Dilution Robot, and software for raw data processing. All non-software (firmware only) systems are operated by Arduino microcontrollers running firmware programmed in C/C++ using the Arduino IDE (Integrative Development Environment) and Microsoft Visual Studio IDE.

The firmware controlling the Vaping Robot operates its pinch valve system, ensuring aerosols only flow forward through the Breathing-Emulator or out into a filter and not back into the reservoir. The firmware also controls the vacuum pump responsible for puffing the E-cigarette. Both of these are controlled by the firmware communicating to the connected 8-channel relay shield through an I2C protocol by bit masking the data packet to active the appropriate relay.

The Dilution Robot also utilizes the firmware to control for timing of pinch valves and vacuums through communicating with the same type of shield. Additionally, the Dilution Robot's firmware is responsible for controlling a linear servo and synchronizing the actuation with the pinch valve timing. The firmware for the linear servo utilizes the Servo.h library for Arduino. The PM Detection System sends raw data from the SPS30 PM Sensor to the serial output of the Arduino utilizing the SPS30-uart library provided by the Sensirion company. The Inhalation Exposure Chamber utilizes temperature, humidity, and CO_2 sensors as inputs for its PID environmental control system and the AutoPID and PWM Frequency libraries to control CO_2 injection and heater temperature. The firmware utilizes the PID and PWM libraries to drive buck converters and binary activated components, including solenoids and relays. The firmware for the Breathing-Emulator steps the Arduino through two arrays of motor commands which control the position of the syringe pump. The first array contains the appropriate number of motor steps while the second array tells the Arduino the rate at which to send the motor step commands. The firmware loops through a series

of checks for non-periodic interrupts while setting up hardware in the background to invoke firmware methods when the calculated timers are reached. When the firmware method is invoked from an expired timer, the method sends a step signal to the motor driver and updates the hardware register timers for the next index as well as updates other meta data and then resumes the main firmware loop.

In addition to firmware, software was developed to create motor command arrays for the Breathing-Emulator and to process the raw data produced by the PM Detection System. The Breathing-Emulator breathing profile generator software was developed in MATLAB and takes volume and flowrate parameters from spirometry flow-volume loops or approximated data as inputs and outputs motor step and step-rate arrays which can be executed by the systems firmware. Data processing software was developed in C++ and MATLAB; a thorough explanation of the data processing workflow can be found in the following section, Data Processing.

Data processing

As the Breathing-Emulator flows aerosols through the PM Sensor, data from the PM Sensor is displayed in the serial monitor. At the completion of each full test cycle, the text on this serial monitor is copied into a text file (.txt) and saved. The data includes quantities over time of mass concentration in $\mu g/m^3$ and numerical count of particles per cm^3. The data samples at $^3/_4$ Hz and captures particles within four different size ranges: 300 nm – 1.0 μm, 1 μm – 2.5 μm, 2.5 μm – 4.0 μm, and 4 μm – 10.0 μm.

A C++ program then scans each text file and processes the data by separating it into concentration or count and storing each dataset in a comma-separated value (.csv) file. Each file includes a column identifying the particle size range. A text file is also automatically generated listing each data file that has been processed.

The rest of the processing is done in MATLAB. A function reads the text file created by the C++ program to know which files to analyze. For each file, it reads the data and stores it in a variable based on particle size. For each particle size, the sum of the smaller particle ranges is subtracted. This results in the sets representing non-overlapping ranges of 300 nm – 1.0 μm, 1.0 μm – 2.5 μm, 2.5 μm – 4.0 μm, and 4.0 μm – 10.0 μm. From here the data is graphed with all four particle sizes for one run on a single graph.

The data are then passed to a subfunction that locates the peak particle counts and concentrations within each trial and marks them on the graph as a vertical line. The number of peaks sought is based on the number of aerosols puffs in the trial. The sum of the particles counted per cm^3 from a puff is calculated by summing the values between the minimum before a peak and the minimum after the same peak in the particles counted per cm^3 data. Particle flow rate, if needed, is determined by multiplying the total particles counted per cm^3 by the total volume displaced of one breath divided by the time of one breath, giving mean particle flow rate per second.

These values are then organized based on grouped datasets, so all trials for the experiment that were completed with the same VEA, nicotine concentration, and breathing profile are placed together. They are exported to Microsoft Excel (.xlsx) files for statistical analysis within GraphPad Prism.

Real-time quantitative analysis of EC aerosols

The E-cigarette Vaping Robot was used with the Dilution Robot and the Breathing-Emulator to reliably aerosolize the E-cigarette liquids, dilute the aerosols, and inhale them into the Particle Detection System for quantitative analysis. The process begins with the Vaping Robot activating a vacuum pump, which acts to puff the E-cigarette and draw aerosol into the Dilution robot's holding reservoir. Once the puff is complete, the aerosol is diluted with the Dilution Robot, the E-cigarette aerosols are inhaled from the reservoir into the Particle Detection System by the retraction of the Breathing-Emulator's plungers and exhaled on the corresponding extension of the plungers. This allows for real-time analysis of particle distributions of a repeatable quantity of inhaled aerosols collected in a manner that is physiologically relevant.

In our studies, E-cigarette liquids containing 50/50 concentration of glycerol (Sigma, Cat. #: W262606) and propylene glycol (Sigma, Cat. #: W294004) was combined with VEA (α-tocopheryl acetate) and/or nicotine to yield VEA concentrations of 0, 1.25, 2.5, and 5% (v/v) (Sigma, Cat. #: T3376) and nicotine concentrations of 0, 0.6, 1.2, and 2.4% (v/v) (Sigma, Cat. #: N3876). All sets of E-liquid samples were generated through serial

dilutions. The E-liquid was used to compare the particle concentrations of the aerosols produced by healthy, obstructive, and restrictive breathing patterns as well as differences between the different ratios of VEA and nicotine with a healthy breathing profile. Tests were conducted using G6 E-cigarette batteries (Halo, 280 mAh 78 mm, ~ 3.7 volts) and Vapor4Life Clearomizers cartridges (808D Thread, 1.3 mL e-liquid volume, 1.8 ohm) cartridges. This yielded a power usage of ~ 7.6 watts. Seven trials were taken for each of the data sets with nine puffs per trial, for a total of 63 puffs per data set.

We took the following items into consideration when performing our studies: (i) Tubing material. We wanted tubing with minimal adsorptive properties on flowing particles that exhibits lowest aerosols condensation. After investigating five different tubing types, we found that PTFE was the most optimal material as it allowed maximal transmission of all four particle sizes being testing through the tubing to the sensor. Transmission was comparable to having no tubing and directly measuring particles coming from EC mouthpiece. Thus, we used PTFE tubing (inner radius: 1 mm) for connections in our system, except at the pinch valves which required Platinum-Cured Silicone tubing (Clippard; inner radius: 400 μm). (ii) Total tubing length. The total tubing length in our platform was approximately 1 m from the site of aerosols generation through the Sensor; much shorter than commercialized smoking/vaping machines (a significant advantage). To minimize any effect that dead volume of the tubing can have on the results, we studied tidal volume fractions – i.e., sample volumes, in the 30-50 mL range that are beyond the total dead volume in our tubing connections (~ 8 mL). (iii) Syringes. The syringes in the Breathing-Emulator were made of glass. They had no impact (e.g., through electrostatic effects) on particle quantities or particle quality (e.g., due to local decompression as aerosols pass through narrow inlets of the syringes), because they were placed past the PM Sensor meaning aerosols that reached the syringes have already been sampled and analyzed. (iv) Sample Volume. To avoid exceeding the upper detection limit of our Sensor, we used sample volumes less than 50 mL. As such, the breathing curves (Figure S4) were not executed to reflect the full tidal volume (500–555 mL). Importantly, this did not affect our analyses, as the endpoint was number concentration – i.e., total particles in each fraction per cm^3. (v) Sensor choice. The choice of Sensor (Sensirion SPS30) in our platform was made after thorough comparison against other commercially available particle detection systems (see discussion). (vi) Robotic Program. When designing our robotic platform, we ensured that EC aerosols only passed the Sensor during inhalation phase and then left the system through a filter. This was to allow us to conduct a more accurate and meaningful analysis.

QUANTIFICATION AND STATISTICAL ANALYSIS

Statistical analysis of particle concentrations, count, or flow rates measured for comparisons of differences in breathing profiles and VEA and nicotine concentrations were tested for a normal distribution with the Shapiro-Wilk test (alpha level 0.05) in GraphPad Prism. None of the experiments had all data sets with a normal distribution. To compare the distributions of the particle concentrations, count, or flow rates the non-parametric Kruskal-Wallis test (alpha level 0.05) was used. Post Hoc analysis was performed with the Dunn's Multiple Comparison Test where differences between the data sets were considered statistically significant when $p < 0.05$ (* $p < 0.05$, ** $p < 0.01$, *** $p < 0.001$, **** $p < 0.0001$). Each data point corresponds to a single aerosols puff, there were nine aerosols puffs per session with 7 sessions total per data set.